JOURNAL OF GEOPHYSICAL RESEARCH, VOL. 114, B03407, doi:10.1029/2008JB005876, 2009

Scaling and paleodepth of compaction bands, Nevada and Utah

Richard A. Schultz[1]

Received 17 June 2008; revised 25 November 2008; accepted 6 January 2009; published 24 March 2009.

[1] Measurements of the lengths and thicknesses of compaction bands in Navajo Sandstone from the Buckskin Gulch, Utah, field site demonstrate displacement-length scaling with a power law exponent of ~0.5, consistent with previous values obtained independently for compaction bands from the Valley of Fire, southern Nevada, site. Compaction energies calculated in this paper for the Utah bands, G_c = 55–120 kJ/m^2, and for the Nevada bands, G_c = 30–60 kJ/m^2, are consistent with those estimated from laboratory experiments despite major differences in band length, thickness, degree of grain fracturing, and remote stress state. Using the field measurements of bands from both sites in the recently proposed inverse relation between the magnitude of remote band-normal compression and compaction band thickness predicts values of band-normal compression of 24–30 MPa for the Utah bands and 31–62 MPa for the Nevada bands. Given that compaction bands at both sites are steeply dipping, these values correspond to a regional tectonic compression oriented subhorizontally at the time of band growth. The results suggest that the compaction bands formed at relatively shallow paleodepths of 0.92–1.3 km at the Utah site and 0.54–1.1 km at the Nevada site, in accord with estimates of the thickness of overlying stratigraphic cover during Sevier-Laramide deformation at both sites. Growth of compaction bands at both field sites was likely facilitated by favorable host rock properties (well-sorted, coarse-grained, high-porosity sandstone sequences) deformed within a thrust faulting tectonic environment.

Citation: Schultz, R. A. (2009), Scaling and paleodepth of compaction bands, Nevada and Utah, *J. Geophys. Res.*, *114*, B03407, doi:10.1029/2008JB005876.

1. Introduction

[2] Compaction bands are a type of deformation band characterized by predominantly closing displacements [e.g., *Mollema and Antonellini*, 1996; *Sternlof et al.*, 2005; *Aydin et al.*, 2006; *Schultz and Fossen*, 2008]. These structures form large-scale networks that impede subsurface fluid flow (petroleum or groundwater) in otherwise porous rock types such as sandstones [e.g., *Sternlof et al.*, 2006] and are widely regarded as one of the least understood types of geologic structure in porous granular rocks [e.g., *Bésuelle and Rudnicki*, 2004; *Holcomb et al.*, 2007; *Rudnicki*, 2007; *Wang et al.*, 2008]. The seminal paper by *Mollema and Antonellini* [1996] documented compaction bands in the field from the Buckskin Gulch site in Utah. Since then, detailed studies of analogous structures in Aztec Sandstone at Valley of Fire State Park, southern Nevada by *Rudnicki and Sternlof* [2005] and *Sternlof et al.* [2005] and laboratory examples of compaction bands [e.g., *Olsson*, 1999; *Issen and Rudnicki*, 2000; *Tembe et al.*, 2006, 2008; *Holcomb et al.*, 2007; *Rudnicki*, 2007] have been compared in an effort to better understand this class of strain localization in porous granular rocks.

[3] The Buckskin Gulch site in south central Utah [*Mollema and Antonellini*, 1996] (Figure 1) is located adjacent to the East Kaibab monocline, which resulted from folding above subjacent normal faults reactivated during the Laramide orogeny as right-oblique thrust faults [*Tindall and Davis*, 1999]. According to *Tindall* [2000], the site is located where structural relief along the monocline is greatest (1200–1600 m). At Buckskin Gulch, the Jurassic Navajo Sandstone [*Doelling and Davis*, 1989] exhibits compaction bands whose subhorizontal exposures (Figure 2) permit accurate measurements of band lengths and thicknesses that, in turn, yield estimates of the depth of formation of the bands.

[4] In this paper, new measurements leading to displacement-length scaling relations of compaction bands from Buckskin Gulch (the "Utah site") are compared to those obtained from Valley of Fire (the "Nevada site") by *Sternlof et al.* [2005] and analyzed by *Rudnicki and Sternlof* [2005], *Rudnicki* [2007], and *Tembe et al.* [2008]. This paper builds on the results from those and related studies, including identification of a critical compaction energy for band propagation [e.g., *Vajdova and Wong*, 2003; *Rudnicki and Sternlof*, 2005; *Tembe et al.*, 2006; *Rudnicki*, 2007], scaling of thickness and band length L according to $\sqrt{L}$ [*Rudnicki*, 2007; *Tembe et al.*, 2008], and an inverse relation between the magnitude of band-normal compression and compaction band thickness [*Tembe et al.*, 2008], which is used in this

[1]Geomechanics–Rock Fracture Group, Department of Geological Sciences and Engineering, University of Nevada, Reno, Nevada, USA.

0148-0227/09/2008JB005876$09.00

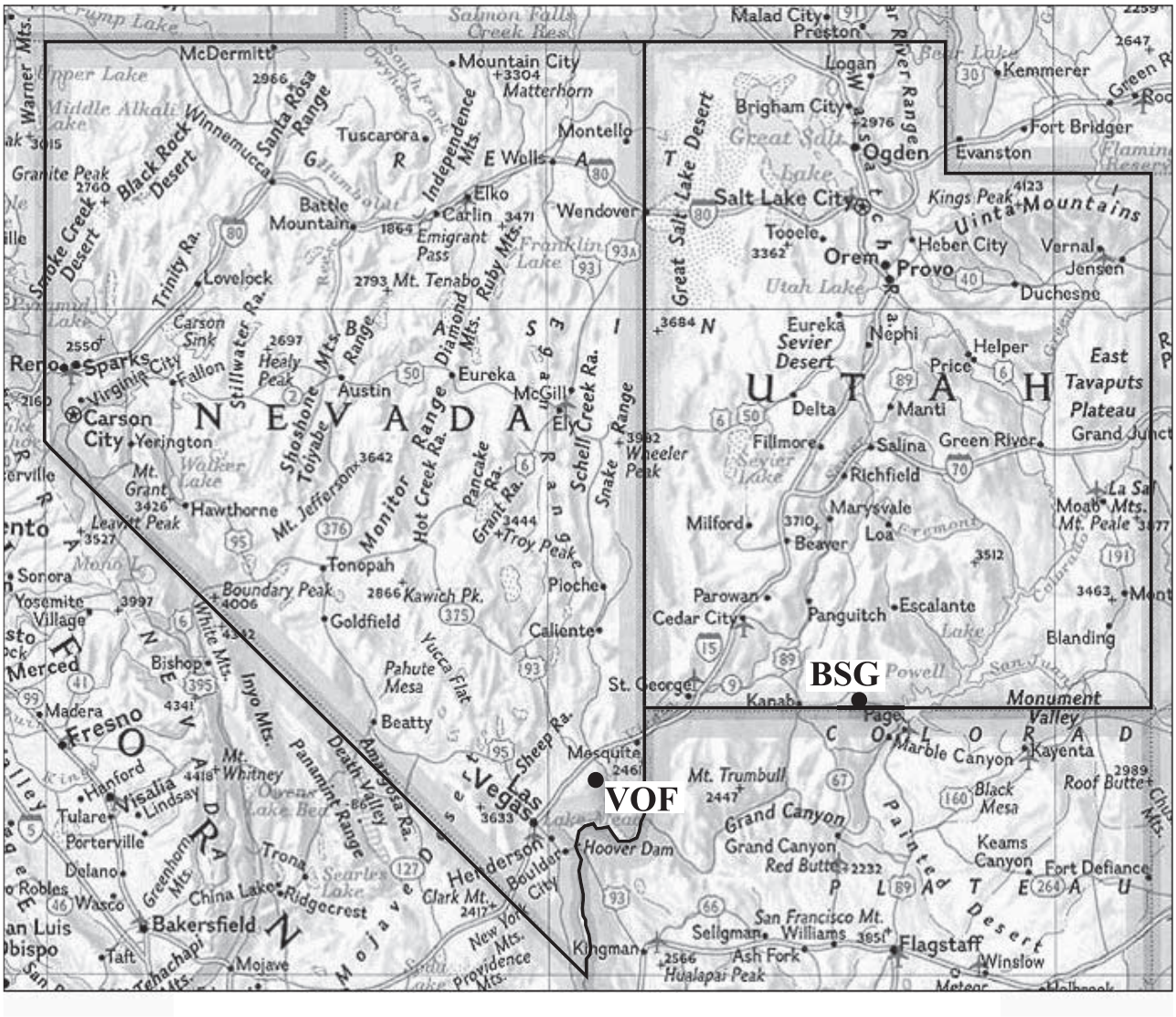

Figure 1. Shaded relief map showing locations of the Valley of Fire site, Nevada (VOF) and Buckskin Gulch site, Utah (BSG). Map base prepared by using TOPO! software (http://www.nationalgeographic. com).

paper to estimate the regional tectonic stress state and paleodepth of band formation at both sides.

2. Compaction Bands at Buckskin Gulch

[5] The Buckskin Gulch locality investigated for this study is a spectacular exposure of subparallel compaction bands whose vertical and lateral extents are well exposed (Figure 2). The bands in this area show a consistent orientation with strike ~N15E and ~55° dip to the east (Figure 3) and with a map view geometry intriguingly reminiscent of compaction bands at the Nevada site [see *Sternlof et al.*, 2005, Figure 1]. Bedding adjacent to the compaction bands can be traced continuously through them without discernable shearing offsets (Figure 4), confirming the field and petrographic observations of *Mollema and Antonellini* [1996] that the bands accommodate primarily compactional strain with little or no shear strain. These observations lend further support to the use of compaction bands as indicators of the orientation of maximum compressive principal stress at the time of their formation [*Mollema and Antonellini*, 1996; *Sternlof et al.*, 2005].

[6] The lengths of compaction bands at the Utah site were measured from a subhorizontal exposure (Figure 2b) by using a steel tape. Band lengths ranged from 0.57 to 15.3 m, with maximum thicknesses, determined from thickness measurements at regular intervals along each band by using a caliper, ranging between 5.1 and 25.4 mm; thickness and length have estimated measurement uncertainties of ±0.2 mm and ±1 mm, respectively. The compaction bands do not exhibit a monotonically varying increase in thickness from tip to band midpoint, but instead are composed of a series of hard-linked segments with lengths of ~15 cm. Compaction band thicknesses therefore exhibit a general increase from ~0 mm at band terminations to maximum values near their midpoints modulated by larger local thicknesses near segment midpoints and smaller thicknesses near segment terminations.

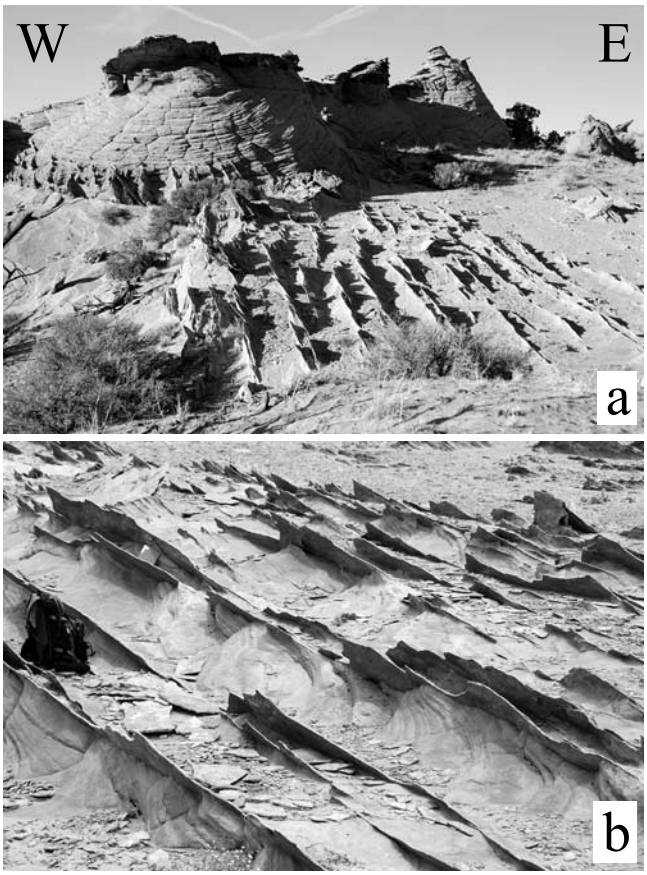

Figure 2. Outcrop expression of compaction bands (exposed as dipping resistant fins) at the Utah site. (a) View to the north showing east dipping bands and their restriction to a ~1 m thick layer visible in the hillside by either lithologic changes or bed-parallel bands. (b) View of compaction bands including those measured for this study; field pack and notebook for scale. GPS coordinate 37°3.170′N, 111°59.445′W, elevation 1495 m.

[7] Measurements of the along-strike thickness variations along compaction bands from the Utah site, shown for the three shortest bands in Figure 5 and in normalized profiles for the same bands in Figure 6, reveal flattened, nonelliptical, plateau-like profiles over a large fraction (i.e., 0.8–0.9 L) of the lengths of the bands. All compaction bands measured for this study show plateau thickness profiles and none cut into the superjacent or subjacent layers, as is evident on Figure 2a.

3. Approach

[8] A total of 8 compaction bands from the Buckskin Gulch site were selected for this analysis; many other bands lacking clear terminations or exhibiting geometric complexities with nearby bands (i.e., low-angle or high-angle linkage) were excluded. The values of band thickness and length used in this paper are the total band dimensions (rather than the semithicknesses and semilengths reported and used by *Tembe et al.* [2008] and others), following the convention in displacement-length scaling studies [e.g., *Watterson*, 1986; *Cowie and Scholz*, 1992; *Dawers et al.*, 1993; *Westaway*, 1994; *Cartwright et al.*, 1995; *Clark and Cox*, 1996; *Fossen and Hesthammer*, 1997; *Gross et al.*, 1997; *Marrett*, 1996; *Olson*, 2003; *Gudmundsson*, 2004; *Xu et al.*, 2006; *Schultz et al.*, 2006; *Fossen et al.*, 2007]. Displacement-length scaling relations for the compaction bands were obtained from values of length L and maximum thickness T_{max}, here associated with the maximum displacement, D_{max}, for consistency with analogous studies of other structures [e.g., *Schultz et al.*, 2006; *Fossen et al.*, 2007] (see discussion in section 4.2).

[9] Previous work showed that compaction bands from the Nevada site scale as $D_{max} \propto \sqrt{L}$ [e.g., *Rudnicki*, 2007; *Tembe et al.*, 2008]. By rearranging equation (6) of *Olson* [2003], the value of fracture toughness K_c and corresponding critical compaction energy G_c (obtained for compaction bands from the Nevada site using an analogous approach by *Rudnicki* [2007]; see Rudnicki's equation (33) and related text) for an isolated compaction band can be calculated by using the measured lengths L and maximum displacements D_{max} from a given compaction band population along with values of Young's modulus E and Poisson's ratio v of the surrounding host rock.

[10] *Olson*'s [2003, equation (6)] analysis assumes that a uniform remote stress state acts on a joint, compaction band, or other structural discontinuity, so that the fracture toughness (or critical stress intensity factor) K_c of the host rock equals the stress intensity factor K at the compaction band tip. However, for nonuniform remote stress states or boundary conditions along a fracture or band, the stress intensity factor may be given succinctly by [e.g., *Broek*, 1983, p. 75; *Anderson*, 1995, p. 60]

$$K = Y\sigma_d\sqrt{\pi a} \tag{1}$$

in which Y is a nondimensional constant or function that quantifies the influence of remote stress state, mechanical interaction, or boundary conditions on the band, σ_d is the

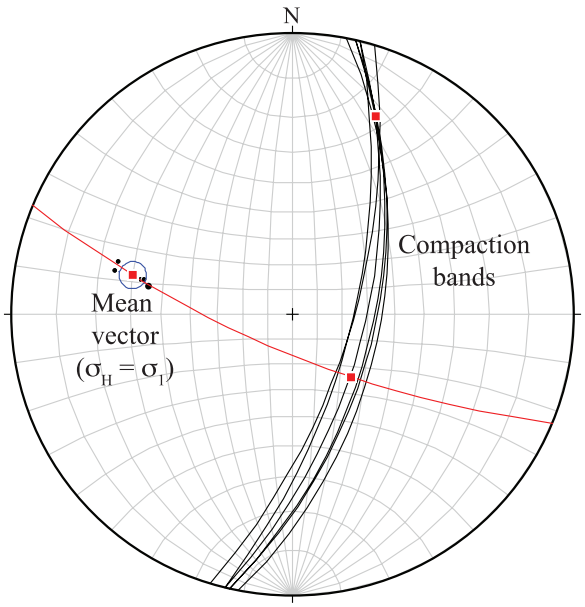

Figure 3. Stereonet of compaction bands at the Buckskin Gulch site. Lower hemisphere, equal-angle projection.

Figure 4. View of compaction bands exposed in cross section at Buckskin Gulch showing continuity of sedimentary bedding in the Navajo Sandstone and consequent lack of discernable shear offsets of bedding along the bands. Pencil along bedding for scale.

driving stress, and $a = L/2$ is the half length of the fracture or band. K may transiently exceed K_c for a given loading geometry, with the condition $K \leq K_c$ being reestablished as a result of fracture or band propagation. Because the fracture toughness is given by $K_c = \sigma_d\sqrt{\pi a}$ [e.g., *Broek*, 1983, p. 121; *Anderson*, 1995, p. 84], equating K with K_c for propagation yields the expression for corrected fracture toughness

$$K_c = \frac{K}{Y} \tag{2}$$

Substituting (2) into equation (6) of *Olson* [2003] with the band's length being defined as $L = 2a$ gives

$$D_{\max} = \left[\frac{\sqrt{8}}{\sqrt{\pi}}\frac{YK_c(1-\nu^2)}{E}\right]\sqrt{L} \tag{3}$$

which has the form

$$D_{\max} = \alpha L^n \tag{4}$$

in which the power law slope is n and the coefficient is α. Equation (3) can be rearranged to obtain

$$K_c = \frac{D_{\max}E\sqrt{\pi}}{Y(1-\nu^2)\sqrt{8L}} \tag{5}$$

Values of K_c thus obtained are then converted to the critical compaction energy G_c by

$$G_c = K_c^2(1-\nu^2)/E \tag{6}$$

assuming linear elastic fracture mechanics and plane strain conditions [e.g., *Broek*, 1983; *Rudnicki and Sternlof*, 2005; *Rudnicki*, 2007].

[11] *Rudnicki* [2007] and *Tembe et al.* [2008] suggested that laboratory and field data were consistent with values of G_c, porosity change $\Delta\phi$, and host rock modulus that varied within relatively narrow ranges. *Tembe et al.* [2008] sug-

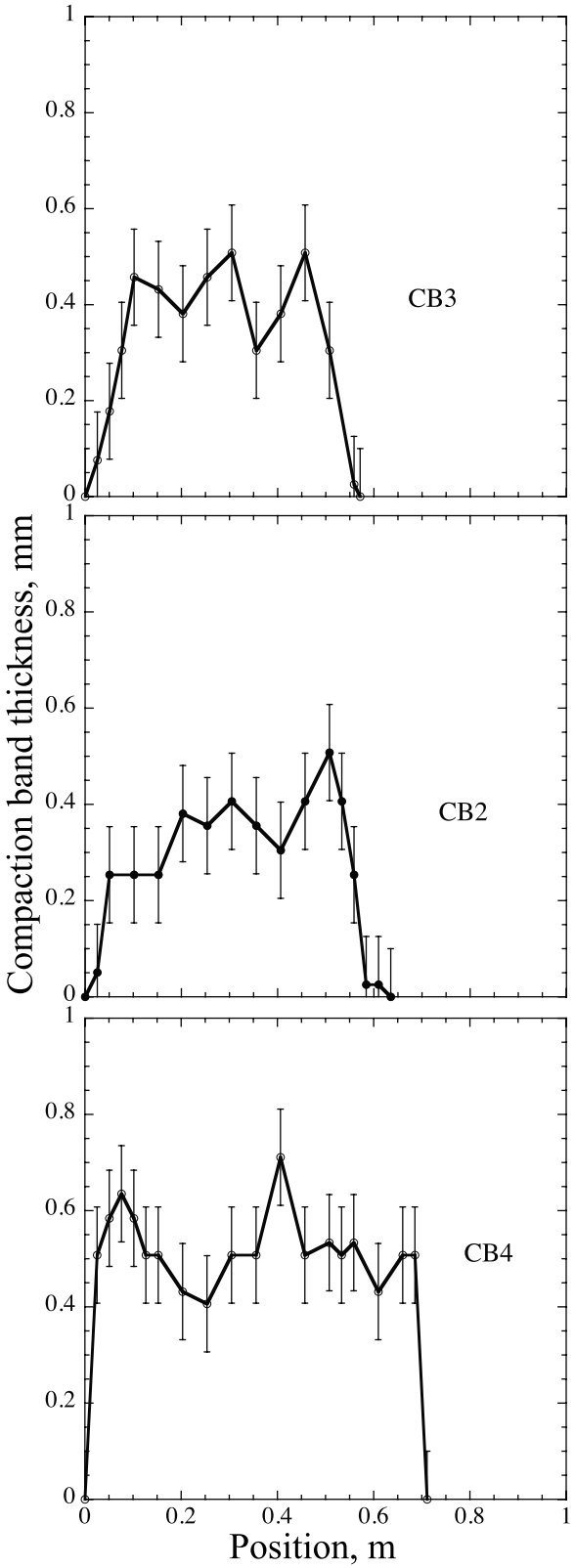

Figure 5. Thickness-length profiles for the three shortest compaction bands (CB2, CB3, and CB4) at the Utah site.

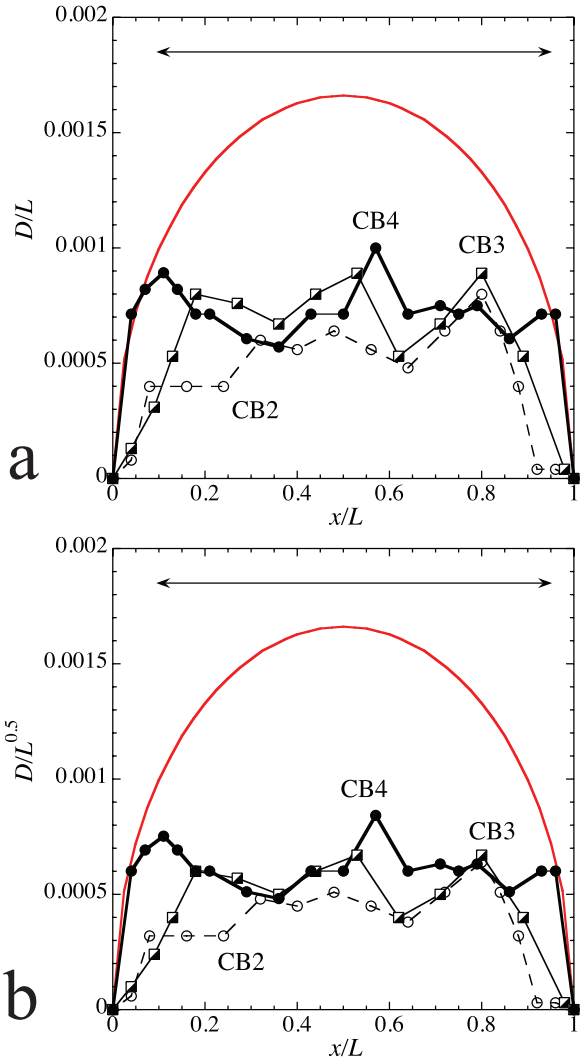

Figure 6. Normalized thickness-length profiles for the three shortest compaction bands at the Utah site; labels as in Figure 5. Ellipses are fit to the normalized band length and show significant reduction in normalized thickness relative to an ideal elliptical thickness variation. (a) Band thickness normalized by band length. (b) Band thickness normalized by square root of band length. Arrows in Figures 6a and 6b indicate approximate range of plateau thickness profiles along the bands.

gested that, for these conditions, the remote band-normal compression σ_n leading to compaction band growth (with compression taken to be positive) was related to band semithickness W (where $W = D_{max}/2$) by

$$\sigma_n = \frac{2G_c}{\pi \Delta\phi W} \tag{7}$$

in which the change in porosity from host rock to compaction band $\Delta\phi$ (with a reduction in porosity relative to the host rock taken as a positive number) is a measure of the inelastic closing strain within the band ε_p, so that wider (thicker) bands require less remote compression to form than thinner bands, all other factors held equal. Inferring compaction band growth under conditions of constant G_c is equivalent to the conditions of constant K_c that can be associated with a $D_{max} \propto \sqrt{L}$ scaling relation as investigated by *Olson* [2003], *Rudnicki* [2007], and *Tembe et al.* [2008].

4. Results and Discussion

4.1. Displacement-Length Scaling

[12] Using data from *Sternlof et al.* [2005], *Rudnicki et al.* [2006], and *Rudnicki* [2007] demonstrated that compaction bands scale in thickness and length according to $T_{max} = A(L')^B$, in which $T_{max} = 2h$ is the measured band thickness and L' is the half length of compaction bands from the Nevada site [see *Rudnicki*, 2007, equation (34)], with $B = n = 0.53$ [see also *Tembe et al.*, 2008, Figure 8]. By combining data from the field sites and from a variety of high-confining pressure triaxial laboratory experiments, and noting that bands in laboratory samples were limited in length by the sample dimensions, *Rudnicki* [2007] and *Tembe et al.* [2008] inferred that compaction bands scale approximately as $n = 0.5$, consistent with *Rudnicki*'s [2007] model for compaction bands growing under conditions of constant compaction energy G_c (see Rudnicki's equation (33)).

[13] The displacement-length data for compaction bands from the Nevada site (digitized from *Sternlof et al.* [2005, Figure 4b]) and the new data collected for this study from the Utah site (Figure 2 and Table 1) are shown in Figure 7. Two separate populations are found, each having slopes approximately equal to $n = 0.5$ within the scatter of the respective data sets [e.g., *Clark and Cox*, 1996] (see Figure 7 for linear regression results and r^2 values). The best fit slope for bands at the Nevada site is $n = 0.51$ (Figure 7), comparable to that found previously for these bands by *Rudnicki* [2007] (i.e., $B = 0.53$). The best fit slope for the Utah bands is $n = 0.44$, which is not significantly different than 0.5 given that some of the measured compaction bands in Utah are characterized by relatively small tip-to-tip spacings and other evidence of short-range mechanical interaction that can reduce population slopes from their baseline value [*Olson*, 2003].

[14] The coefficients of the power law fits to these compaction band populations, $\alpha = 0.0019$ m$^{1/2}$ for compaction bands from the Nevada site and 0.0063 m$^{1/2}$ for bands from the Utah site (Figure 7), are significantly different (i.e., 0.0063/0.0019 = 3.3). Compaction bands at the Utah site are consistently ~3 times thicker than bands of equivalent length at the Nevada site, as evident on Figure 7 and as

Table 1. Displacement Length Data for Utah Compaction Bands

L (m)	D_{max}[a] (m)	D_{max}/L	$D_{max}/\sqrt{L}$
0.572	0.00508	8.9×10^{-3}	2.1×10^{-3}
0.635	0.00508	8.0×10^{-3}	3.4×10^{-3}
0.711	0.00711	1.0×10^{-2}	8.4×10^{-3}
1.74	0.00635	3.7×10^{-3}	4.8×10^{-3}
5.05	0.00889	1.8×10^{-3}	4.0×10^{-3}
6.86	0.0121	1.8 t 10^{-3}	4.6×10^{-3}
7.91	0.0218	2.8×10^{-3}	7.8×10^{-3}
15.29	0.0254	1.7×10^{-3}	6.5×10^{-3}

[a]Value corresponds to the maximum value of thickness measured in the field for each band.

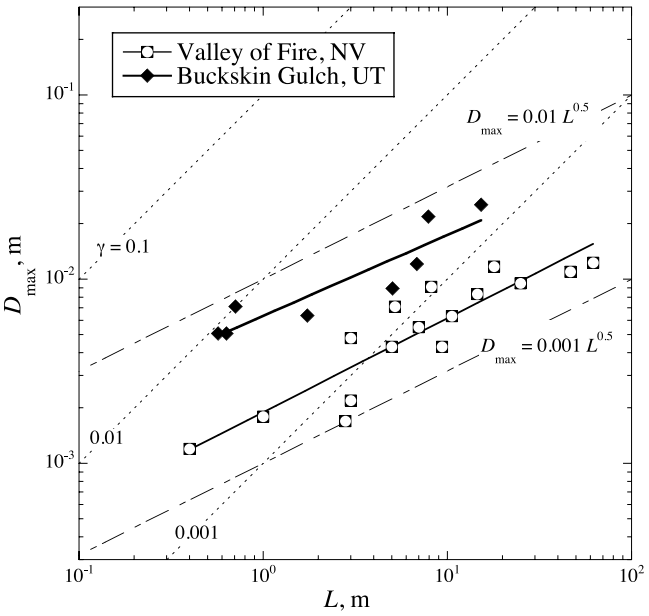

Figure 7. Displacement-length scaling relations for compaction bands. Lines of constant slope are shown: $n = 1$ (appropriate for faults [*Clark and Cox*, 1996; *Schultz et al.*, 2006], shown for reference), dotted, with $D_{max}/L = \gamma$; $n = 0.5$, dashed. Bands from the Nevada site show $D_{max} = 0.0019\ L^{0.51}$, $r^2 = 0.76$; bands from the Utah site show $D_{max} = 0.0063\ L^{0.44}$, $r^2 = 0.83$, with measurement uncertainties contained within the data symbols.

expressed in their respective population coefficients (Figure 7), implying a factor of 3 variation in Young's modulus [e.g., *Gudmundsson*, 2004] and/or fracture toughness [*Olson*, 2003] between the two field sites. Because the grain sizes and porosities from both sites are approximately the same, Young's modulus E and Poisson's ratio ν should be approximately equal in (3) for either site [e.g., *Chang et al.*, 2006]. The difference in scaling coefficient between the two compaction band populations therefore implies an increase, for bands from the Utah site, in either the fracture toughness K_c or the parameter Y (see equation (5)) of about a factor of 3 relative to bands from the Nevada site. This difference is explored in section 4.2.

4.2. Compaction Energies

4.2.1. Nevada Site

[15] Using values of Young's modulus and Poisson's ratio of $E = 20$ GPa and $\nu = 0.2$, respectively for Aztec Sandstone [*Sternlof et al.*, 2005; *Rudnicki and Sternlof*, 2005] with $Y = 1.0$ in (3), the closing-mode fracture toughness is approximately $K_c = 25$ MPa m$^{1/2}$ for the Nevada bands. Using (6), this value becomes $G_c = 30$ kJ/m^2, in excellent agreement with the values of $G_c = 10–60$ kJ/m^2 obtained independently by using the J integral approach by *Rudnicki and Sternlof* [2005] (and assuming normal stresses of 13–54 MPa calculated by *Sternlof et al.* [2005], perhaps rounded by *Rudnicki and Sternlof* [2005] to 10–60 MPa, and which are reevaluated in section 4.3.1). Using the same approach (i.e., equation (3)) as that used in this paper, *Rudnicki* [2007] found $2h = A(L')^B$ with A giving $G_c = 30$ kJ/m^2, assuming the same values of E and ν (converted by Rudnicki into a shear modulus of 8.33 GPa) and in good agreement with the value of 40 kJ/m^2 calculated by *Rudnicki and Sternlof* [2005] using the value of band-normal compression from *Sternlof et al.* [2005] of 40 MPa.

[16] The three-dimensional shapes of compaction bands at the Nevada site were taken to be subcircular or disc-shaped by *Sternlof et al.* [2005]; the value of Y for this case, $2/\pi$ [e.g., *Willemse et al.*, 1996; *Schultz and Fossen*, 2002], when used in (5) with the power law scaling coefficient obtained in Figure 7 leads to values of $K_c = 40$ MPa m$^{1/2}$ and $G_c = 76.8$ kJ/m^2, comparable to or somewhat larger than the previous estimates of *Rudnicki and Sternlof* [2005] and *Rudnicki* [2007]. However, because band shape was assumed to be indefinitely large in the vertical dimension, consistent with plane strain conditions, in *Rudnicki*'s [2007] derivation and *Tembe et al.*'s [2008] analysis, we do not consider the shapes of compaction bands from either site further, and set $Y = 1.0$ in (5) for bands from the Nevada site in the remainder of this paper.

[17] Recent work on compaction bands relates the inelastic closing displacement u_c to the band thickness T through the inelastic closing (compactional) strain within the band ε_p [*Sternlof et al.*, 2005; *Rudnicki*, 2007; *Tembe et al.*, 2008] so that the maximum closing displacement $u_{c\,max}$ would be related to the maximum measured thickness T_{max} by

$$u_{c\,max} = 2\varepsilon_p W = \varepsilon_p T_{max} \tag{8}$$

Petrographic observations of compaction bands indicate that plastic distortion of grain shapes and pervasive grain cracking also contribute to the compactional strain accommodated by a compaction band in addition to porosity reduction due to a tighter grain packing geometry [*Mollema and Antonellini*, 1996; *Sternlof et al.*, 2005], so that the inelastic closing strain across a compaction band ε_p incorporates all three components (i.e., grain distortion, grain cracking, and grain rearrangement).

[18] Setting ε_p equal to the reduction in porosity $\Delta\phi$ within the band relative to the host rock for the Nevada site [e.g., *Sternlof et al.*, 2005; *Tembe et al.*, 2008] leads to $u_{c\,max} = 0.1\ T_{max}$. Because the value of K_c obtained from the band scaling relations (5) varies linearly with band thickness, substituting values of the implied closing displacement $u_{c\,max}$ for D_{max} in (5) would lead to values of $K_c = 2.5$ MPa m$^{1/2}$ and $G_c = 0.3$ kJ/m^2, a compaction energy 2 orders of magnitude smaller than those calculated by *Rudnicki and Sternlof* [2005], *Rudnicki* [2007] (who equated the maximum band thickness T_{max} with the maximum closing displacement $2h$ in his calculation; see Rudnicki's equations (33), (34), and related text), and *Tembe et al.* [2008]. The J integral calculation of *Rudnicki and Sternlof* [2005] was not specific about how, or when, porosity reduction along a band may have been related to the local magnitude of band-normal compression (which likely increased with position from its far-field value as the band tip was approached) or about whether the value of ε_p used (0.1 in the work by Rudnicki and Sternlof) was appropriate to that associated with compaction band propagation, as noted by Rudnicki and Sternlof, casting some uncertainty on the value of ε_p that should be used in calculating G_c from the measured values of band thickness. Given these caveats and the remarkable consistency between the values of G_c

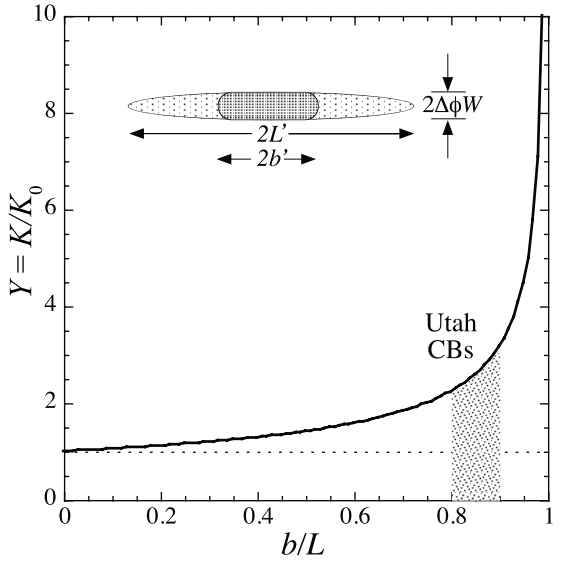

Figure 8. Plot of equation (9) showing increase in stress intensity factor K at the tip of a compaction band with increasing flattening of its thickness profile relative to K_0 at the tip of a band having an elliptical (unflattened) thickness profile. Parameters in equation (9) defined in inset and the text.

obtained in this paper (using $T_{max} = D_{max}$) and the previous independent results of *Rudnicki and Sternlof* [2005] and *Rudnicki* [2007], the maximum band thicknesses are used as D_{max} in (5) instead of inelastic closing displacements $u_{c\,max}$, with the values of band-normal compression calculated by using (7) thereby potentially representing upper limits to σ_n.

4.2.2. Utah Site

[19] Using the values of E = 20 GPa and v = 0.2, given that the Navajo Sandstone is correlative with the Aztec Sandstone [*Marzolf*, 1983], with Y = 1.0 in (5) gives values of K_c = 100–150 MPa m$^{1/2}$ and G_c = 483–1068 kJ/m^2 for the Utah bands, a critical compaction energy G_c that is a factor of 9 larger than for bands at the Nevada site. Because G_c in this approach depends on the value of fracture toughness K_c at the time of compaction band propagation, and because $K_c = K$ (the stress intensity factor at the compaction band tip) during band propagation, the larger values of G_c for the Utah bands relative to the values for the Nevada bands likely imply larger values of K in (1) for the Utah bands on the order of $\sqrt{9} = 3$.

[20] *Rudnicki* [2007] showed that K for compaction bands that have flatter thickness profiles than the elliptical ones reported from the Nevada site by *Sternlof et al.* [2005] would be larger than K for compaction bands having elliptical thickness profiles. Following *Rudnicki* [2007], the relationship is given by

$$\frac{K}{K_0} = \frac{\left\{\sqrt{\frac{\pi}{(L' - b')}\left[\frac{E\Delta\phi W}{2(1+\nu)(1-\nu)}\right]}\right\}}{\left[\frac{E\Delta\phi W}{2(1-\nu)}\sqrt{\frac{\pi}{L'}}\right]} = \frac{1}{\sqrt{1 - \frac{b'}{L'}}} = Y \quad (9)$$

where b' is taken as the half length of plateau, constant closing displacements (corresponding to compactional dislocations in his model) along the band of half length $a = L$' (Figure 8, inset), K_0 is the (closing mode) stress intensity factor for a band having an elliptical thickness profile (i.e., $b = 0$ and $Y = 1.0$; smooth curves in Figure 6). Using the ratio of b/L of 0.8–0.9 inferred for the Utah bands (Figure 6, arrows), the relation in (9) implies that the parameter Y in (3) and (5) may be approximately equal to 3.

[21] Setting Y = 3 in (5) gives K_c = 33–50 MPa m$^{1/2}$, corresponding to a compaction energy of G_c = 55–120 kJ/m^2. These values of compaction energy are consistent with those for other compaction bands, both from the field (Nevada site; *Rudnicki and Sternlof*, 2005]) and from the laboratory [*Rudnicki*, 2007; *Tembe et al.*, 2006, 2008] that have approximately $2 < G_c < 60$ kJ/m^2.

4.3. Magnitude of Remote Compression During Band Growth

4.3.1. Nevada Site

[22] The magnitude of compressive stress normal to compaction bands at the Nevada site is calculated here by using equation (7) with values of E = 20 GPa, ν = 0.2, compactional strain across the bands of $\varepsilon_p = \Delta\phi$ = 0.1 [*Sternlof et al.*, 2005], and maximum band semithicknesses $D_{max}/2 = W$ = 6.15 mm. The initial values, listed in Table 2, are σ_n = 10–62 MPa for G_c = 10–60 kJ/m^2. Values calculated from smaller band lengths correspond to band-normal compressive stresses in excess of 100 MPa (Figure 9), which are in the range of laboratory values (although the band semithicknesses at the Nevada site are a factor of 5 larger) but which are inconsistent with the relatively shallow depths inferred for band growth at the Nevada site, as discussed in section 4.4.1.

[23] For the vertically dipping compaction bands at the Valley of Fire, Nevada site, the remote compressive principal stresses associated with the formation of compaction bands were estimated by *Sternlof et al.* [2005] to be between 13 and 54 MPa. However, those values apparently assume dry conditions (no pore fluid pressure [see also *Tembe et al.*, 2008, Table 5, footnote a]. For example, using an average dry rock density ρ of 2250 kg m^{-3} [*Sternlof et al.*, 2005], gravitational acceleration g = 9.8 m s^{-2}, and a minimum stratigraphic thickness of 0.6 km [*Sternlof et al.*, 2005], the vertical principal stress at the top of the Navajo Sandstone at

Table 2. Calculated Paleostresses σ_n and Paleodepths z for Compaction Bands

Sandstone	D_{max} (mm)	G_c (kJ/m^2)	σ_n[a] (MPa)	μ	Band Dip (deg)	z (km)
Aztec (NV)	12.3	10	10.35	-	0	-
	12.3	30	**31.06**	0.85	0	**0.54**
	12.3	60	**62.11**	0.85	0	**1.08**
Navajo (UT)	25.4	55	13.78	-	55	-
	25.4	120	30.08	0.85	55	1.16
	25.4	120	**30.08**	0.6	55	**1.33**
	25.4	90[b]	**23.8**	0.85	55	**0.92**

[a]Values calculated by using equation (7) with E = 20 GPa and ν = 0.2 [*Sternlof et al.*, 2005]. Bold values for σ_n and z correspond to the likely ranges inferred from stratigraphic thicknesses given band dip angles and the thrust-faulting environment (see Figures 11 and 12) and to the bold error bars on Figure 9.

[b]Value estimated from Figure 12 for z to match the minimum stratigraphic thickness (0.92 km).

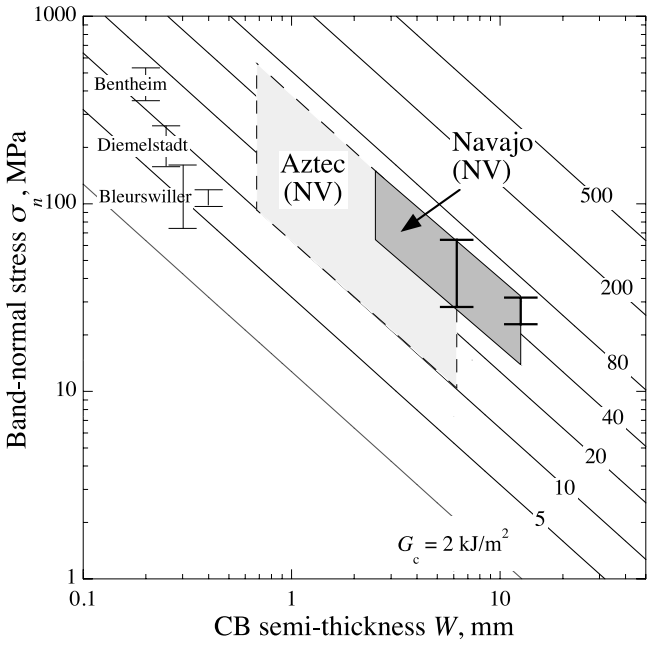

Figure 9. Magnitude of regional compression calculated by using equation (7) as a function of compaction band semithickness. Contours of G_c calculated by using (7), over the range of W, with $\Delta\phi = 0.1$. Values for triaxial laboratory samples (Bentheim, Diemelstadt, and Bleurswiller sandstones) from *Tembe et al.* [2008]. Ranges for Aztec [*Rudnicki and Sternlof*, 2005] and Navajo sandstones (shaded polygons) given by the range of band semithicknesses and values of G_c calculated from the band population statistics. Range for Navajo Sandstone at the Utah site (G_c = 20–100 kJ/m^2) plots at $G_c/2$ given $\Delta\phi = 0.2$ for those bands (see text). Horizontal bars and arrows indicate ranges of regional compressive stress calculated for both sites from stratigraphic thicknesses (see text).

the Nevada site is calculated to be $\sigma_v = \rho gz = (2250)(9.8)(0.6)/1000 = 13.23$ MPa. Assuming the value of $\sigma_1/\sigma_3 = \sigma_H/\sigma_v = 2$ used for a thrust-faulting environment at the Nevada site by *Sternlof et al.* [2005], thereby implying a rather low maximum ("static") friction coefficient for the host sandstone of $\mu = 0.35$, yields an upper bound on the horizontal compression normal to the compaction bands, at the maximum stated stratigraphic thickness of 1.2 km, of $\sigma_H = 2\sigma_v = 2\rho gz = 2(2250)(9.8)(1.2)/1000 = 52.9$ MPa, which is close to the upper bound of 54 MPa given by *Sternlof et al.* [2005] that again assumes dry rock density in the deforming sandstone.

[24] Using an average value of stratigraphic cover thickness of 0.9 km and an average dry rock density ρ of 2250 kg m^{-3}, *Sternlof et al.* [2005] calculated values for $\sigma_v = \sigma_3$ of (2250)(9.8)(0.9) = 20 MPa and $\sigma_H = \sigma_1 = 2\sigma_3$ of 40 MPa which are within the stated range of 13–54 MPa. Assuming hydrostatic pore fluid conditions instead, consistent with the field evidence for an active groundwater environment in the Aztec Sandstone around the time of compaction band formation [*Eichhubl et al.*, 2004] during Cretaceous Sevier orogeny thrusting [*Bohannon*, 1983; *Flodin and Aydin*, 2004], and therefore an effective rock density of $\rho_{rock} - \rho_{water} = 2250 - 1000 = 1250$ kg m^{-3}, the effective vertical principal stress for the stated range of stratigraphic thicknesses at the Nevada site, 0.6–1.2 km, would be σ_v = 7.35–14.7 MPa. Applying values of q (see section 4.4) of 3.1 and 4.68, 435 corresponding to static friction coefficients μ of 0.4 and 0.85, respectively, yields revised values of $\sigma_1 = q\sigma_3 = \sigma_n = 22$–70 MPa normal to compaction bands at the Nevada site (see equation (10)) inferred from the stratigraphic constraint.

4.3.2. Utah Site

[25] According to *Mollema and Antonellini* [1996], the change in porosity for the Utah compaction bands was a decrease from 20 to 25% in the host rock to "a few percent or less" within the bands, corresponding to $\Delta\phi$ of approximately 0.2, a value twice that reported for the Nevada bands by *Sternlof et al.* [2005]. The magnitude of compressive stress normal to compaction bands at the Utah site is calculated here by using equation (7) with values of E = 20 GPa, $\nu = 0.2$, compactional strain across the bands of $\varepsilon_p = \Delta\phi = 0.2$, and maximum band semithicknesses $D_{max}/2 = W = 12.7$ mm. The values, listed in Table 2, are σ_n = 14–30 MPa for G_c = 55–120 kJ/m^2. Because $\Delta\phi = 0.2$ for the Utah bands, the range in σ_n for the Utah bands shown on Figure 9 plots at values corresponding to $G_c/2$. This implies that compaction bands having greater reductions in porosity relative to the host rock, and therefore greater values of compactional strains [*Rudnicki*, 2007; *Tembe et al.*, 2008] across them, scale in $\sigma_1 = \sigma_n$ and depth (see section 4.4.2) as bands growing under conditions of reduced G_c.

4.4. Paleodepths for Band Formation

[26] The magnitudes of remote compressive stress normal to the compaction bands at the Utah and Nevada sites, calculated in the previous section from band thicknesses by using (7), are evaluated in this section by comparing them to the corresponding values of tectonic stress obtained from estimates of the thickness of stratigraphic units overlying the Navajo formation at the time of band formation.

[27] Given that both field sites are in thrust faulting environments [*Tindall and Davis*, 1999; *Sternlof et al.*, 2005], the stress state in Aztec or Navajo Sandstone is given by the Coulomb criterion written by using remote principal effective stresses [*Jaeger and Cook*, 1979, p. 97; *Price and Cosgrove*, 1990, p. 26]

$$\sigma_1 = q\sigma_3 \tag{10}$$

in which $q = (\sqrt{\mu^2 + 1} + \mu)^2$ with μ being the average static (or maximum [see *Marone*, 1998]) friction coefficient. Typical values of static and dynamic friction coefficients for crustal rocks are μ = 0.2–0.8 [*Paterson and Wong*, 2005, pp. 166–170; *Jaeger et al.*, 2007, p. 70], with strength given by values of static friction at the high end of the range. Setting $\mu = 0.6$ (corresponding to a representative friction coefficient for rock [*Sibson*, 1994]) gives $q = 3.12$. Typical ranges of friction coefficient μ of 0.4–0.85 lead to values of q = 2.2–4.68.

[28] For thrust faulting, σ_1 is the maximum horizontal compressive principal stress σ_H, and σ_3 is the vertical compressive principal stress σ_v, and compaction bands that are normal to the maximum compression, so that $\sigma_1 = \sigma_n$, would

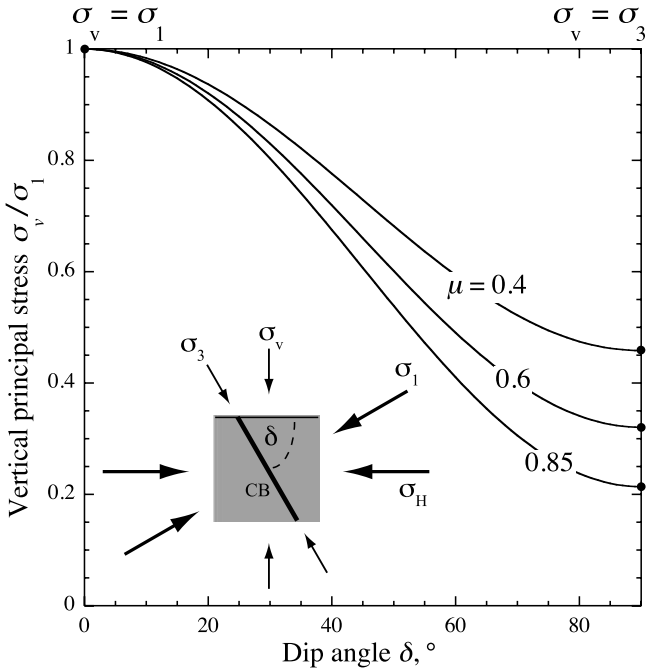

Figure 10. Plot of equation (11) showing variation in band-normal compression σ_n with band dip angle δ. For horizontal bands ($\delta = 0°$) the band-normal compression is vertical; for vertical bands ($\delta = 90°$), σ_n is horizontal so that the vertical compressive principal stress σ_v is related to it through the friction coefficient μ.

be vertical (i.e., a dip angle of 90°). For nonvertical bands, the normal stress resolved on a band having an arbitrary dip angle δ (see Figure 10 inset) is given by

$$\sigma_n = \left(\frac{\sigma_1 + \sigma_3}{2}\right) + \left(\frac{\sigma_1 - \sigma_3}{2}\right)\cos(2\delta) \qquad (11)$$

so that the vertical principal stress acting on the compaction band σ_v is given by

$$\sigma_v = \sigma_1\left[\left(\frac{q+1}{2q}\right) + \left(\frac{q-1}{2q}\right)\cos(2\delta)\right] \qquad (12)$$

Equation (12) is plotted in Figure 10. For horizontal compaction bands (dip angle δ of 0°) the normal stress on the band is the maximum compressive principal stress σ_1 and also the vertical stress σ_v, as would be the case in a triaxial laboratory experiment with bands that form normal to the cylindrical sample axis. For vertical bands such as those at the Nevada site [*Sternlof et al.*, 2005] (dip angle δ of 90°), the normal stress is horizontal and $\sigma_v = \sigma_3$ with the magnitude of the vertical principal stress depending on the friction coefficient (μ or q) of the host rock (equation (10)). For bands having dip angles between these extremes, such as those at the Utah site, the normal stress on the band is σ_1 with the value of σ_v again modulated by δ and q. The paleodepth z, in m, for compaction bands having arbitrary dip angles is given by

$$z = \frac{\sigma_1}{2\rho g q}[(q+1) + (q-1)\cos(2\delta)] \qquad (13)$$

Using values of remote compression normal to the bands, $\sigma_n = \sigma_1$, obtained from (7) in (13) gives estimates of the paleodepths for compaction band growth at the two field sites.

4.4.1. Nevada Site

[29] The values of band-normal compression at the Nevada site calculated from equation (7), σ_n = 10–62 MPa, compare well with those inferred by converting σ_v calculated from the stratigraphic thickness estimate (0.6–1.2 km) into σ_H associated with a thrust faulting environment, with $\sigma_1 = \sigma_H = \sigma_n$ = 22–70 MPa and vertically dipping compaction bands (Figure 11). For G_c = 30–60 kJ/m^2 and μ = 0.85, the paleodepth corresponding to a band-normal compression of $\sigma_H = \sigma_n$ = 31–62 MPa would be z = 0.54–1.08 km (bold values in Table 2 and error bars at W = 6.15 mm on Figure 9 (upper right corner of "Aztec" polygon)), in excellent agreement with the stratigraphic cover estimate. Although the curves for the full range of compaction energies inferred for the Nevada site, 10–60 kJ/m^2, predict too broad a range of paleodepths depending on the value of μ chosen (see Table 2, bold values), the curve for μ = 0.4 and G_c = 60 kJ/m^2 (Figure 11) also is consistent with a paleodepth of ~1.2 km.

4.4.2. Utah Site

[30] A Paleocene Laramide age of thrusting was inferred for the Utah site by *Tindall and Davis* [1999]. On the basis of a detailed analysis of lithospheric plate motions relative

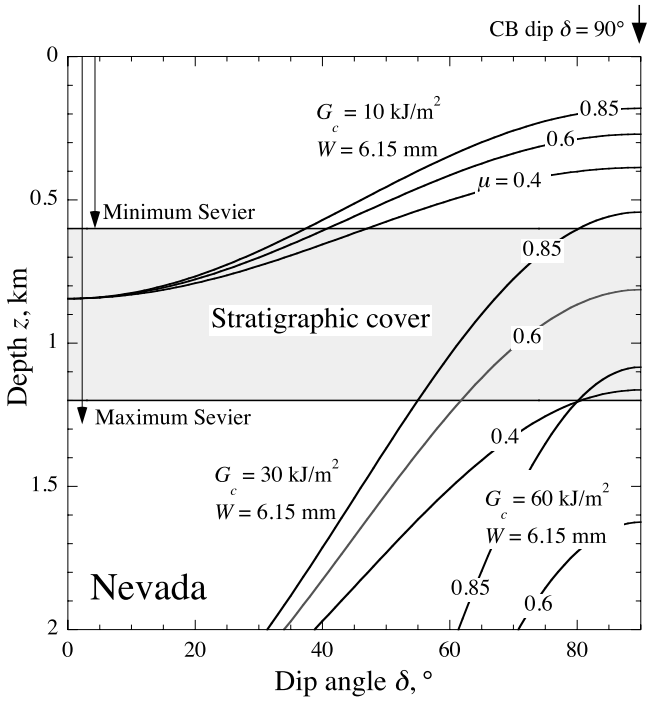

Figure 11. Paleodepth of compaction bands at the Valley of Fire, Nevada, site (Aztec Sandstone) as a function of band semithicknesses obtained by using equation (13). Shaded area corresponds to estimates of paleodepths of bands inferred from thickness of stratigraphic cover during compaction band formation (z = 600–1200 m). Paleodepths of compaction bands that fit the stratigraphic range (calculated from $\sigma_v = \rho g z$) for range of friction coefficient ($0.4 \leq \mu \leq 0.85$) shown for $\delta = 90°$ (arrow at right edge).

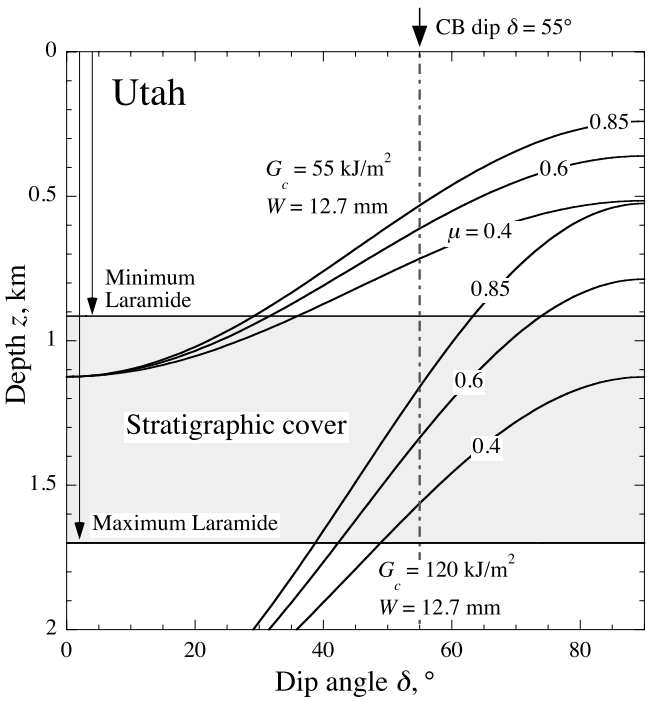

Figure 12. Paleodepth of compaction bands at the Buckskin Gulch, Utah, site (Navajo Sandstone) as a function of band semithicknesses obtained by using equation (13). Shaded area as in Figure 11 but with z = 915–1700 m. Paleodepths of compaction bands determined as in Figure 11 but for $\delta = 55°$ (arrow and dashed vertical line).

to a fixed hot spot reference frame, *Engebretson et al.* [1984] concluded that the Laramide orogeny was associated with a high rate of convergence between western North America and the subducting Farallon plate [*Coney*, 1978; *Cross and Pilger*, 1978] along with shallow subduction [e.g., *Coney*, 1972] of rapidly younging [e.g., *Livaccari et al.*, 1981; *Henderson et al.*, 1984] oceanic lithosphere at the trench beginning at ~74 Ma, corresponding to Paleocene time [see also *Engebretson et al.*, 1985]. *Tindall and Davis* [1999] note that Upper Cretaceous Kaiparowits and Wahweap formations were involved in anticlinal folding along the East Kaibab monocline north of the Utah site, suggesting a Late Cretaceous to Paleocene age of deformation there and perhaps at the Utah site as well. Adopting an age of ~74 Ma for the onset of thrust-fault-related compaction bands at the Utah site provides an estimate of the thickness of stratigraphic cover above the deformed Jurassic Navajo Sandstone that leads, in turn, to estimates of the vertical principal stress σ_v at the top of the Navajo at the time of band formation at the Nevada and Utah sites.

[31] The thickness of overlying strata at the Utah site is estimated here by summing the thicknesses of units above the deformed Jurassic Navajo Sandstone through the Paleocene section (see *Hintze*'s [1988] chart 97 for the stratigraphic section in the Kanab-Alton area), corresponding to a thickness of 915–1700 m (shaded area on Figure 12). This thickness corresponds to an overburden stress σ_v of 11.2–20.8 MPa assuming an effective rock density of 1250 kg m^{-3} that includes hydrostatic pore water pressure.

[32] Paleodepths of z = 1.16–1.56 km for compaction bands from the Utah site are consistent with the bands dipping at $\delta = 55°$ (Figures 2 and 3) in a thrust faulting stress state assuming G_c = 120 kJ/m^2 for μ = 0.4–0.85 (Figure 12). Predicted paleodepths calculated by assuming G_c = 55 kJ/m^2 underestimate the stratigraphic thickness estimate by about a factor of 2. The minimum thickness of 0.92 km is met for G_c = 90 kJ/m^2 and μ = 0.85, for σ_n = 23.8 MPa (Table 2), implying that the band-normal compression for bands from the Utah site was approximately σ_n = 24–30 MPa (bold values in Table 2 and error bars at W = 12.7 mm on Figure 9 (upper right corner of "Navajo" polygon)).

4.5. Driving Stress and Critical Pressure for Band Growth

[33] For compaction bands having an elliptical thickness profile, the driving stress σ_d leading to band propagation varies with band length according to $K_c = \sigma_d\sqrt{\pi a} = \sigma_d\sqrt{\pi L'}$ [*Rudnicki*, 2007]. For compaction bands having a plateau thickness profile associated with a constant compactional dislocation along the flat-topped portion of the band (see Figure 9 inset for parameters), $K_c = \sigma_d\sqrt{\pi(L' - b')}$, following *Rudnicki* [2007]. Rearranging the latter expression and noting that $L = 2a$ gives

$$\sigma_d = \frac{\sqrt{2}K_c}{\sqrt{\pi(L-b)}} \tag{14}$$

Using the range of compaction band lengths from the Nevada site [*Sternlof et al.*, 2005], L = 1–62 m, and a fracture toughness obtained in this paper of K_c = 25 MPa m$^{1/2}$ with b = 0 in (14), the driving stress during compaction band growth was σ_d = 2.5–20.0 MPa (Table 3). Using the values of band-normal compression consistent with the stratigraphic bounds of σ_n = 31–62 MPa obtained for the longest (L = 62 m) and thickest (D_{max} = 12.3 mm) compaction bands, the driving stress was approximately σ_d = 2.5 MPa at the time the bands at the Nevada site stopped propagating. At the Utah site, the values of compaction band length (L = 0.57–15.3 m) and fracture toughnesses (K_c = 33–50 MPa m$^{1/2}$), with b/L = 0.85 in (14) imply driving stresses of σ_d = 17.4–26.3 MPa (Table 3) for the longest compaction bands.

[34] The driving stress acting on a compaction band can be expressed as $\sigma_d = (\sigma_r - \sigma_i)$ [*Schultz and Fossen*, 2002; *Rudnicki*, 2007], where $\sigma_r = \sigma_n$ is the value of far-field (remote) compressive stress normal to the band plane and σ_i is the resistance to compaction, which likely corresponds either to the compactive yield strength C^* or to the critical pressure for grain crushing P^* of the host sandstone near the band tip. Compaction bands at the Utah and Nevada sites are characterized by porosity reduction related to grain reorganization, with grain cracking being a minor component [*Mollema and Antonellini*, 1996; *Sternlof et al.*, 2005], implying that $\sigma_i = C^*$ for these bands. On the other hand, observations of significant grain fracturing and crushing in the triaxial laboratory experiments [e.g., *Holcomb et al.*, 2007] suggest that σ_i might be interpreted instead as the

Table 3. Driving Stress and Compactive Yield Strength for Compaction Bands

Sandstone	L (m)	K_c (MPa m$^{1/2}$)	σ_d (MPa)	σ_n (MPa)	σ_i (MPa)	P^*[a] (MPa)	σ_i/P^*
Aztec (NV)	62.0	25	2.5	31	28.5	66	0.43
	62.0	25	2.5	62	59.5	66	0.9
Navajo (UT)	15.3	33	17.4	30	12.6	20–27[b]	0.47–0.63
	15.3	50	26.3	30	3.7	20–27	0.14–0.19

[a]Assumes andydrous conditions.
[b]Range calculated for porosity values of 20–25% and average grain size of 0.55 mm [*Mollema and Antonellini*, 1996].

critical pressure for grain crushing, P^* [*Zhang et al.*, 1990; *Wong et al.*, 2004] for those bands. The onset of localized compaction C^* marks the beginning of a capped yield envelope for the host rock [e.g., *Wong et al.*, 1997]. Assuming an elliptical [e.g., *Wong et al.*, 1997] or teardrop-shaped [e.g., *Davis and Selvadurai*, 2002; *Borja and Aydin*, 2004] yield envelope, the ratio of C^* to the critical pressure to initiate grain crushing P^* [*Zhang et al.*, 1990; *Wong and Baud*, 1999; *Wong et al.*, 2004] should be in the range of $C^*/P^* \geq 0.5$.

[35] The values of band-normal compression σ_n calculated in this paper from (7) are related to σ_i through the driving stress (equation (14)) by

$$\sigma_i = \sigma_n - \frac{\sqrt{2}K_c}{\sqrt{\pi(L-b)}} \tag{15}$$

The critical pressure for quartz grains in a sandstone is given by [*Zhang et al.*, 1990; *Wong et al.*, 2004]

$$P^* = \frac{\Gamma}{(\phi R)^{1.5}} \tag{16}$$

in which ϕ is host rock porosity, R is the average grain radius (in mm), and Γ is a material property parameter approximately equal to 1 MPa mm$^{3/2}$ for quartz grains in Hertzian contact. Although this relation is defined for anhydrous conditions, experimental work indicates that P^* is reduced for water-saturated porous sandstones by a factor that ranges from <5% for a nearly pure quartz sandstone to more than 50% for sandstones rich in feldspar [e.g., *Wong and Baud*, 1999; *Tembe et al.*, 2008].

[36] Using porosity and average grain size for Aztec Sandstone of 0.245 and 0.25 mm, respectively [*Sternlof et al.*, 2005], $P^* = 66$ MPa. The calculated values of σ_i for the Nevada bands, 28.5 and 59.5 MPa (Table 3), are 43 to 90% of P^*, suggesting that σ_i is consistent with C^* for both values of normal stress, 31.1 and 62.1 MPa, associated with a paleodepth of 0.54 to 1.08 km (Table 2, bold values).

[37] According to *Mollema and Antonellini* [1996], the grain size in layers of Navajo Sandstone in which the (thick) compaction bands are found ranges from 0.3 to 0.8 mm, for a mean grain size of $R = 0.55$ mm. Assuming the range of porosities given by Mollema and Antonellini of 20–24%, $P^* = 20$–27 MPa for Navajo Sandstone (Table 3). The calculated values of σ_i for the Utah bands, 3.7 and 12.6 MPa (Table 3), are 14–63% of P^* calculated for the Navajo Sandstone, perhaps implying an association between nonuniform compaction along the bands (i.e., $b/L > 0$) and values of C^*/P^* less than 0.5. The analysis suggests that values of driving stress σ_d and compactive yield strength σ_i for compaction bands may be estimated from the displacement-length scaling relations of the band population in combination with band orientations (i.e., dip angle) and an independent stratigraphic constraint.

[38] Numerical experiments recently reported by *Wang et al.* [2008] utilize $\sigma_i = P^* = 200$ MPa. *Tembe et al.* [2006, Figure 5] suggest that P^* in laboratory experiments on Bentheim and Berea sandstones is on the order of 400 MPa. Because the magnitudes of σ_i are comparable to σ_n, the driving stresses for compaction band growth may also be relatively small in these laboratory and numerical experiments, perhaps similar to the values inferred for the field examples of compaction bands from the Nevada and Utah sites.

5. Conclusions

[39] Displacement-length scaling of compaction bands at the two known field sites exhibit square root of length scaling, consistent with previous inferences of band growth related to a critical compaction energy G_c. Magnitudes of the regional tectonic horizontal compressive stress normal to the compaction bands and paleodepths of band formation estimated from population scaling for both sites are comparable and consistent with estimates of stratigraphic thickness at the time of band growth. The large magnitudes of band-normal compression at relatively shallow depths in the crust at both sites, <1–2 km, are associated with steeply dipping compaction bands forming in a well-sorted, coarse-grained, high-porosity sandstone within a thrust faulting tectonic regime.

[40] **Acknowledgments.** Chris Okubo kindly introduced the author to the Utah site. Thanks to John Rudnicki and Teng-fong Wong for reprints and preprints of their work on compaction bands, and to Rick Allmendinger for the use of his stereonet program (version 6.6.3X). Thorough and thoughtful reviews by two anonymous referees, and comments from Associate Editor John Spray, led to substantial improvements in the final paper for which the author is grateful. This work was supported by NASA's Planetary Geology and Geophysics Program, in collaboration with Shell International Exploration and Production, Inc. and Orion Geomechanics (http://www.oriongeomechanics.com).

References

Anderson, T. L. (1995), *Fracture Mechanics: Fundamentals and Applications*, 2nd ed., CRC Press, Boca Raton, Fla.

Aydin, A., R. I. Borja, and P. Eichhubl (2006), Geological and mathematical framework for failure modes in granular rock, *J. Struct. Geol.*, *28*, 83–98, doi:10.1016/j.jsg.2005.07.008.

Bésuelle, P., and J. W. Rudnicki (2004), Localization: Shear bands and compaction bands, in *Mechanics of Fluid-Saturated Rocks*, edited by Y. Guéguen and M. Boutéca, pp. 219–321, Elsevier, Amsterdam.

Bohannon, R. G. (1983), Mesozoic and Cenozoic tectonic development of the Muddy, North Muddy, and northern Black Mountains, Clark County, Nevada, in *Tectonic and Stratigraphic Studies in the Eastern Great Basin*, edited by D. M. Miller, V. R. Todd, and K. A. Howard, *Mem. Geol. Soc. Am.*, vol. 157, pp. 125–148.

Borja, R. I., and A. Aydin (2004), Computational modeling of deformation bands in granular media. I. Geological and mathematical framework,

Comput. Methods Appl. Mech. Eng., *193*, 2667–2698, doi:10.1016/j.cma.2003.09.019.
Broek, D. (1983), *Elementary Engineering Fracture Mechanics*, 3rd ed., Martinus Nijhoff, Boston, Mass.
Cartwright, J. A., B. D. Trudgill, and C. S. Mansfield (1995), Fault growth by segment linkage: An explanation for scatter in maximum displacement and trace length data from the Canyonlands grabens of SE Utah, *J. Struct. Geol.*, *17*, 1319–1326, doi:10.1016/0191-8141(95)00033-A.
Chang, C., M. D. Zoback, and A. Khaksar (2006), Empirical relations between rock strength and physical properties in sedimentary rocks, *J. Petrol. Sci. Eng.*, *51*, 223–237, doi:10.1016/j.petrol.2006.01.003.
Clark, R. M., and S. J. D. Cox (1996), A modern regression approach to determining fault displacement-length scaling relationships, *J. Struct. Geol.*, *18*, 147–152, doi:10.1016/S0191-8141(96)80040-X.
Coney, P. J. (1972), Cordilleran tectonics and North America plate motion, *Am. J. Sci.*, *272*, 603–628.
Coney, P. J. (1978), Mesozoic-Cenozoic Cordilleran plate tectonics, in *Cenozoic Tectonics and Regional Geophysics of the Western Cordillera*, edited by R. B. Smith and G. P. Eaton, *Mem. Geol. Soc. Am.*, vol. 152, pp. 33–50.
Cowie, P. A., and C. H. Scholz (1992), Physical explanation for the displacement-length relationship of fault using a post-yield fracture mechanics model, *J. Struct. Geol.*, *14*, 1133–1148, doi:10.1016/0191-8141(92)90065-5.
Cross, T. A., and R. H. Pilger Jr. (1978), Constraints on absolute motion and plate interaction inferred from Cenozoic igneous activity in the western United States, *Am. J. Sci.*, *278*, 865–902.
Davis, R. O., and A. P. S. Selvadurai (2002), *Plasticity and Geomechanics*, Cambridge Univ. Press, Cambridge, U. K.
Dawers, N. H., M. H. Anders, and C. H. Scholz (1993), Growth of normal faults: Displacement-length scaling, *Geology*, *21*, 1107–1110, doi:10.1130/0091-7613(1993)021<1107:GONFDL>2.3.CO;2.
Doelling, H. H., and F. D. Davis (1989), The geology of Kane County, Utah, *Bull.*, *124*, Utah Dep. of Nat. Resour., Salt Lake City.
Eichhubl, P., W. L. Taylor, D. D. Pollard, and A. Aydin (2004), Paleo-fluid flow and deformation in the Aztec Sandstone at the Valley of Fire, Nevada: Evidence for the coupling of hydrogeologic, diagenetic, and tectonic processes, *Geol. Soc. Am. Bull.*, *116*, 1120–1136, doi:10.1130/B25446.1.
Engebretson, D. C., A. Cox, and G. A. Thompson (1984), Correlation of plate motions with continental tectonics: Laramide to Basin-Range, *Tectonics*, *3*, 115–119, doi:10.1029/TC003i002p00115.
Engebretson, D. C., A. Cox, and R. G. Gordon (1985), Relative motions between oceanic and continental plates in the Pacific Basin, *Spec. Pap. Geol. Soc. Am.*, *206*, 59 pp.
Flodin, E. A., and A. Aydin (2004), Evolution of a strike-slip fault network, Valley of Fire State Park, southern Nevada, *Geol. Soc. Am. Bull.*, *116*, 42–59, doi:10.1130/B25282.1.
Fossen, H., and J. Hesthammer (1997), Geometric analysis and scaling relations of deformation bands in porous sandstone, *J. Struct. Geol.*, *18*, 1–16.
Fossen, H., R. A. Schultz, Z. K. Shipton, and K. Mair (2007), Deformation bands in sandstone: A review, *J. Geol. Soc.*, *164*, 755–769, doi:10.1144/0016-76492006-036.
Gross, M. R., G. Gutiérrez-Alonzo, T. Bai, M. A. Wacker, and K. B. Collinsworth (1997), Influence of mechanical stratigraphy and kinematics on fault scaling relations, *J. Struct. Geol.*, *19*, 171–183, doi:10.1016/S0191-8141(96)00085-5.
Gudmundsson, A. (2004), Effects of Young's modulus on fault displacement, *C. R. Geosci.*, *336*, 85–92, doi:10.1016/j.crte.2003.09.018.
Henderson, L. J., R. G. Gordon, and D. C. Engebretson (1984), Mesozoic aseismic ridges of the Farallon plate and southward migration of shallow subduction during the Laramide orogeny, *Tectonics*, *3*, 121–132, doi:10.1029/TC003i002p00121.
Hintze, L. F. (1988), Geologic history of Utah, *Spec. Publ., 7*, Brigham Young Univ., Geol. Stud., Provo Utah.
Holcomb, D., J. W. Rudnicki, K. A. Issen, and K. Sternlof (2007), Compaction localization in the Earth and the laboratory: State of the research and research directions, *Acta Geotech.*, *2*, 1–15, doi:10.1007/s11440-007-0027-y.
Issen, K. A., and J. W. Rudnicki (2000), Conditions for compaction bands in porous rock, *J. Geophys. Res.*, *105*, 21,529–21,536, doi:10.1029/2000JB900185.
Jaeger, J. C., and N. G. W. Cook (1979), *Fundamentals of Rock Mechanics*, 3rd ed., Chapman and Hall, New York.
Jaeger, J. C., N. G. W. Cook, and R. W. Zimmerman (2007), *Fundamentals of Rock Mechanics*, 4th ed., Blackwell, Oxford, U. K.
Livaccari, R. F., K. Burke, and A. M. C. Sengör (1981), Was the Laramide orogeny related to subduction of an oceanic plateau?, *Nature*, *289*, 276–278, doi:10.1038/289276a0.
Marone, C. (1998), Laboratory-derived friction laws and their application to seismic faulting, *Annu. Rev. Earth Planet. Sci.*, *26*, 643–696, doi:10.1146/annurev.earth.26.1.643.
Marrett, R. (1996), Aggregate properties of fracture populations, *J. Struct. Geol.*, *18*, 169–178, doi:10.1016/S0191-8141(96)80042-3.
Marzolf, J. E. (1983), Changing wind and hydraulic regimes during deposition of the Navajo and Aztec sandstones, Jurassic (?) southwestern United States, in *Eolian Sediments and Processes*, edited by M. E. Brookfield and T. S. Ahlbrandt, pp. 635–660, Elsevier, Amsterdam.
Mollema, P. N., and M. A. Antonellini (1996), Compaction bands: A structural analog for anti-mode I cracks in aeolian sandstone, *Tectonophysics*, *267*, 209–228, doi:10.1016/S0040-1951(96)00098-4.
Olson, J. E. (2003), Sublinear scaling of fracture aperture versus length: An exception or the rule?, *J. Geophys. Res.*, *108*(B9), 2413, doi:10.1029/2001JB000419.
Olsson, W. A. (1999), Theoretical and experimental investigation of compaction bands in porous rock, *Geophys. Res. Lett.*, *104*, 7219–7228.
Paterson, M. S., and T.-f. Wong (2005), *Experimental Rock Deformation—The Brittle Field*, 2nd ed., Springer, Berlin, Germany.
Price, N. J., and J. W. Cosgrove (1990), *Analysis of Geological Structures*, Cambridge Univ. Press, Cambridge, U. K.
Rudnicki, J. W. (2007), Models for compaction band propagation, in *Rock Physics and Geomechanics in the Study of Reservoirs and Repositories*, edited by C. David and M. Le Ravalec-Dupin, *Geol. Soc. Spec. Publ.*, vol. 284, pp. 107–125.
Rudnicki, J. W., and K. R. Sternlof (2005), Energy release model of compaction band propagation, *Geophys. Res. Lett.*, *32*, L16303, doi:10.1029/2005GL023602.
Rudnicki, J. W., S. Tembe, and T.-f. Wong (2006), Relation between width and length of compaction bands in porous sandstones, *Eos Trans. AGU*, *87*(52), Fall Meet. Suppl., Abstract T43A-1633.
Schultz, R. A., and H. Fossen (2002), Displacement-length scaling in three dimensions: The importance of aspect ratio and application to deformation bands, *J. Struct. Geol.*, *24*, 1389–1411, doi:10.1016/S0191-8141(01)00146-8.
Schultz, R. A., and H. Fossen (2008), Terminology for structural discontinuities, *AAPG Bull.*, *92*, 853–867, doi:10.1306/02200807065.
Schultz, R. A., C. H. Okubo, and S. J. Wilkins (2006), Displacement-length scaling relations for faults on the terrestrial planets, *J. Struct. Geol.*, *28*, 2182–2193, doi:10.1016/j.jsg.2006.03.034.
Sibson, R. H. (1994), An assessment of field evidence for 'Byerlee' friction, *Pure Appl. Geophys.*, *142*, 645–662, doi:10.1007/BF00876058.
Sternlof, K. R., J. W. Rudnicki, and D. D. Pollard (2005), Anticrack inclusion model for compaction bands in sandstone, *J. Geophys. Res.*, *110*, B11403, doi:10.1029/2005JB003764.
Sternlof, K. R., M. Karimi-Fard, D. D. Pollard, and L. J. Durlofsky (2006), Flow and transport effects of compaction bands in sandstone at scales relevant to aquifer and reservoir management, *Water Resour. Res.*, *42*, W07425, doi:10.1029/2005WR004664.
Tembe, S., V. Vajdova, T.-f. Wong, and W. Zhu (2006), Initiation and propagation of strain localization in circumferentially notched samples of two porous sandstones, *J. Geophys. Res.*, *111*, B02409, doi:10.1029/2005JB003611.
Tembe, S., P. Baud, and T.-f. Wong (2008), Stress conditions for the propagation of discrete compaction bands in porous sandstone, *J. Geophys. Res.*, *113*, B09409, doi:10.1029/2007JB005439.
Tindall, S. E. (2000), The Cockscomb segment of the East Kaibab monocline: Taking the structural plunge, in *Geology of Utah's Parks and Monuments*, edited by D. A. Sprinkel, T. C. Chidsey Jr., and P. B. Anderson, *Utah Geol. Assoc. Publ.*, vol. 28, pp. 1–15.
Tindall, S. E., and G. H. Davis (1999), Monocline development by oblique-slip fault-propagation folding: The East Kaibab monocline, Colorado Plateau, Utah, *J. Struct. Geol.*, *21*, 1303–1320, doi:10.1016/S0191-8141(99)00089-9.
Vajdova, V., and T.-f. Wong (2003), Incremental propagation of discrete compaction bands: Acoustic emission and microstructural observations on circumferentially notched samples of Bentheim, *Geophys. Res. Lett.*, *30*(14), 1775, doi:10.1029/2003GL017750.
Wang, B., Y. Chen, and T.-f. Wong (2008), A discrete element model for the development of compaction localization in granular rock, *J. Geophys. Res.*, *113*, B03202, doi:10.1029/2006JB004501.
Watterson, J. (1986), Fault dimensions, displacements and growth, *Pure Appl. Geophys.*, *124*, 365–373, doi:10.1007/BF00875732.
Westaway, R. (1994), Quantitative analysis of populations of small faults, *J. Struct. Geol.*, *16*, 1259–1273, doi:10.1016/0191-8141(94)90068-X.
Willemse, E. M. J., D. D. Pollard, and A. Aydin (1996), Three-dimensional analyses of slip distributions on normal fault arrays with consequences for fault scaling, *J. Struct. Geol.*, *18*, 295–309, doi:10.1016/S0191-8141(96)80051-4.

Wong, T.-f., and P. Baud (1999), Mechanical compaction of porous sandstone, *Oil Gas Sci. Technol.*, *54*, 715–727, doi:10.2516/ogst:1999061.
Wong, T.-f., C. David, and W. Zhu (1997), The transition from brittle faulting to cataclastic flow in porous sandstones: Mechanical deformation, *J. Geophys. Res.*, *102*, 3009–3025, doi:10.1029/96JB03281.
Wong, T.-f., C. David, and B. Menéndez (2004), Mechanical compaction, in *Mechanics of Fluid-Saturated Rocks*, edited by Y. Guéguen and M. Boutéca, pp. 55–114, Elsevier, Amsterdam.
Xu, S.-S., A. F. Nieto-Samaniego, S. A. Alaniz-Álvarez, and L. G. Velasquillo-Martínez (2006), Effect of sampling and linkage on fault length and length-displacement relationship, *Int. J. Earth Sci.*, *95*, 841–853, doi:10.1007/s00531-005-0065-3.
Zhang, J., T.-f. Wong, and D. M. Davis (1990), Micromechanics of pressure-induced grain crushing in porous rocks, *J. Geophys. Res.*, *95*, 341–352, doi:10.1029/JB095iB01p00341.

R. A. Schultz, Geomechanics–Rock Fracture Group, Department of Geological Sciences and Engineering/172, University of Nevada, Reno, NV 89557-0138, USA. (schultz@mines.unr.edu)